

Narrow Band *Chandra* X-ray Analysis of Supernova Remnant 3C 391

Yang Su ^{*} and Yang Chen

Department of Astronomy, Nanjing University, Nanjing 210093, China

Received 2004 month day; accepted 2004 month day

Abstract We present the narrow-band and the equivalent width (EW) images of the thermal composite supernova remnant (SNR) 3C 391 for the X-ray emission lines of elements Mg, Si & S using the *Chandra* ACIS Observational data. These EW images reveal the spatial distribution of the emission of the metal species Mg, Si & S in the remnant. They have clumpy structure similar to that seen from the broadband diffuse emission, suggesting that they are largely of interstellar origin. We find an interesting finger-like feature protruding outside the southwestern radio border of the remnant, which is somewhat similar to the jet-like Si structure found in the famous SNR Cas A. This feature may possibly be the debris of the jet of ejecta which implies an asymmetrical supernova explosion of a massive progenitor star.

Key words: ISM: supernova remnants — X-rays: ISM — X-rays: individual (3C 391) — ISM: lines and bands

1 INTRODUCTION

3C 391 (G31.9+0.0) is an irregular mixed-morphology (Rho & Peter 1996, Chen & Slane 2001) supernova remnant (SNR) which generates bright thermal X-ray emission interior and has a faint X-ray rim. The remarkable radio shell which extends from the northwest (NW) to the southeast (SE) shows that the SNR has broken out of a dense region into an adjacent region on lower density (Reynolds & Moffett 1993). 3C 391 is similar to W28, W44, IC 443 and other SNRs (Reach & Rho 1998) in that they interact with molecular clouds, characterized by the hydroxyl radical emission (Green et al. 1997; Yusef-Zadeh et al. 2003).

^{*} E-mail: ysu@nju.edu.cn

We observe SNR 3C 391 with the Advanced CCD Imaging Spectrometer (ACIS) on board the *Chandra* observatory and unveil a highly clumpy structure in broadband (0.3-1.5, 1.5-3, 3-7, and 0.3-7 keV) X-rays (Chen et al. 2004, hereafter CSSW04). The spectrum analysis favors a solar abundance for the X-ray emitting gas. In the broadband images, a faint emission of gas seems to spill out of the south-western (SW) radio border which corresponds to the blast wave there. The nature of such a spill out leakage of gas is unclear.

Here we report the results from the narrow-band and the equivalent width (EW) images of the X-ray emission lines for metal species Mg, Si and S using the observation of the ACIS detector on board the *Chandra* X-ray Observatory. The EW maps for the element species Mg, Si, and S allow us to distinguish the more detailed structure by the less continuum contamination, and might also be useful to understand the line emission distributions and variations throughout the remnant generally. The narrow-band images and the EW images are similar to the whole broadband (0.3-7 keV) X-ray emission in the overall elongated morphology. The narrow-band and EW images reveal, apart from the clumpy structure similar to that seen in the broadband image, a finger-like protrusion in Si & S lines outside the SW radio border. The physical significance of this protrusion then is discussed.

2 DATA

Here we revisit the *Chandra* ACIS observational data of SNR 3C 391 (ObsID 2786) with an exposure of 61.5 ks, which was used by CSSW04 for spatially resolved spectroscopic analysis. The observation was carried out with the ACIS-S3 CCD chip using very faint mode. The level 1 raw event data were reduced to generate a level 2 event file using standard threads in the *Chandra* Interactive Analysis of Observations (CIAO) software package version 3.1. During the course of the reprocessing, we filtered bad grades, applied good time intervals (GTI) correction, and removed significant background flares to reduce the contamination. Also, the overall light curve was examined for possible contamination from time-variable background. The reduced data, with the effective exposure of 60.6 ks, are used for subsequent narrow-band analysis.

3 NARROW-BAND AND EQUIVALENT-WIDTH IMAGES

We present the exposure-corrected broadband (0.3-7 keV) raw image of 3C 391 in Fig. 1a, in which many clumpy features as discussed by CSSW04 can be discerned. The overexposed broadband image of the SW region shown in Fig. 1b highlights the spill-out X-ray emitting gas mentioned in CSSW04.

In the *Chandra* ACIS spectrum (1-3 keV) of 3C 391 (Fig. 2), one can see that substantial X-ray emission comes from metal lines, such as Mg He α (1.35 keV), Si He α (1.85

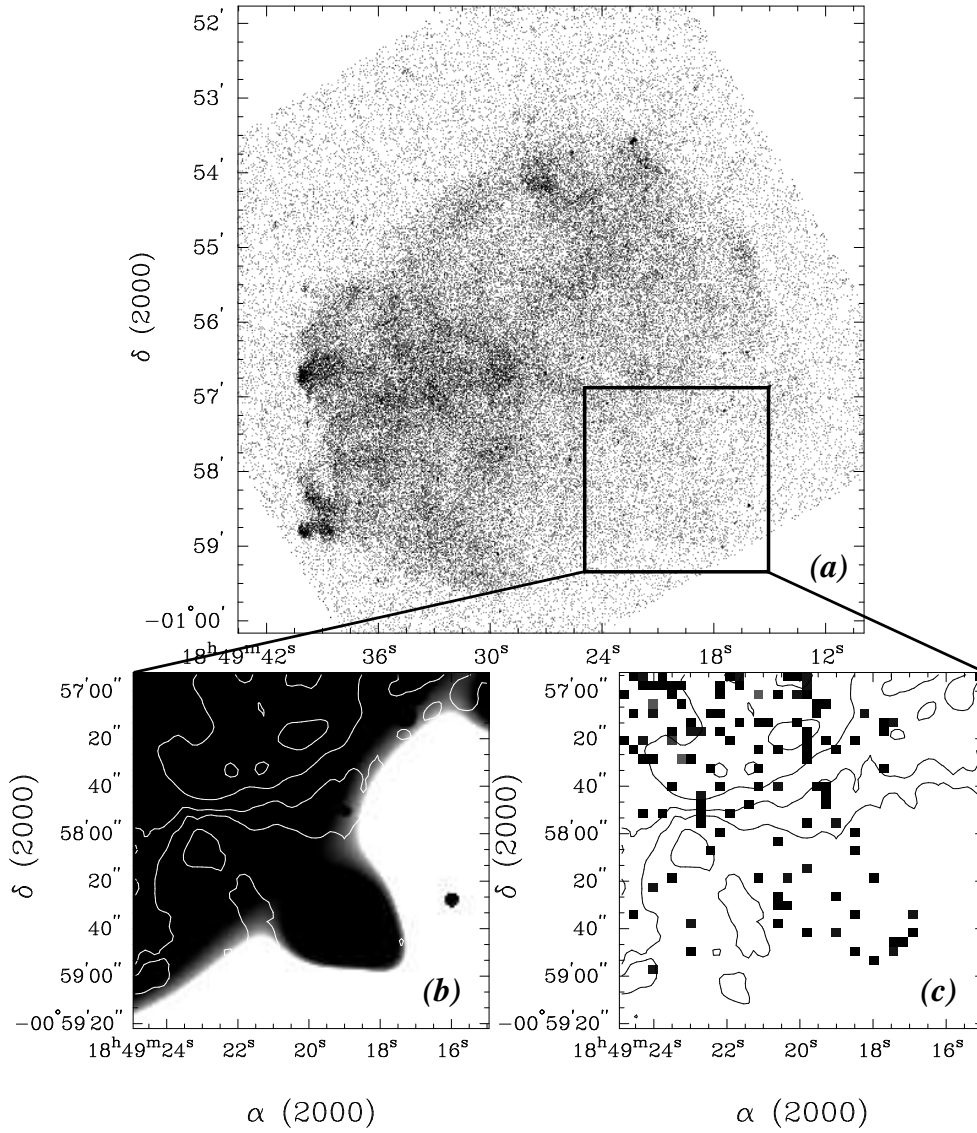


Fig. 1 (a). Broadband (0.3-7 keV) ACIS S3 raw image of 3C 391. The SW box ($2.5' \times 2.5'$) indicates the region of the spill-out emission (CSSW04). (b). Adaptively smoothed broadband (0.3-7 keV) image (with S/N ratio of 3) of the SW region. The overlaid 1.5 GHz radio solid contours are at 1.5, 3.19, 8.25, and 16.69×10^{-3} Jy/beam (from Moffett & Reynolds 1994). (c). Unsmoothed line-to-continuum ratio (i.e., EW) image for Si in the same region as in (b), overlaid with the 1.5 GHz radio contours with the same levels as in (b). All the X-ray maps used here are exposure-corrected and plotted with a square-root scaling.

keV), and S He α (2.46 keV). With respect to the broadband map, the narrow-band and the EW line-emission maps will show us the morphological and positional details of the emissions from various metal species.

The narrow-band Mg He α (1.2-1.5 keV), Si He α (1.7-2.0 keV), and S He α (2.3-2.6 keV) images (without subtraction of the continuum contribution) is given in Fig. 3. These three narrow-band images have been adaptively smoothed (using CIAO tool *csmooth* with signal-to-noise ratio of 3) and exposure-corrected. The clumpy structure in narrow-band is similar to that seen in the broadband images (CSSW04). Comparing these narrow-band images with the overlaid 1.5 GHz radio contours (from Moffett & Reynolds 1994), we find that the Si and S images (Fig. 3b and 3c) show a finger-like protrusion, positional consistent with the broadband “spill-out” emission (Fig. 1b) in the southwest.

Next, we want to see the spatial distribution of the emission purely of metal species Mg, Si, and S. Because X-ray line and thermal continuum emissivities are both proportional to the emission measure, the line emission in a region of low surface brightness may still be strong relative to the continuum. The line emission map with the correction for underlying continuum may help to reveal the spatial distribution of metal species. Therefore we produced the EW maps, essentially following the methods and steps described by Hwang et al. (2000) and Park et al. (2002, 2003).

We selected photons corresponding to each particular spectral line by identifying appropriate energy bands, as shown in table 1. In mapping the line emission, we subtracted the underlying continuum from each line image and then get a ratio image relative to the continuum. Since Mg He α line is blended with Fe L complex, we combine them together to increase statistic photons. First, we extracted images in two narrower energy bands on the both sides of each line profile (Fig. 2) and minimize the contamination from the line emission. The underlying continuum was calculated by linearly interpolating from the two sides. The estimated continuum flux was integrated over the selected line width and subtracted from the line emission. Then, the continuum-subtracted line in intensity was divided by the estimated continuum on a pixel-by-pixel basis to generate EW images for each element. In order to avoid noise in this process and decrease the poor photon statistic uncertainty, we have set EW values to zero where the integrated continuum flux is greater than the line flux and the intensity of the result is too low or too high. The EW images for Mg and Si were constructed with 4'' pixels and smoothed by a Gaussian with $\sigma = 12''$, and that for S was constructed with 8'' pixels and smoothed by a Gaussian with $\sigma = 16''$. The gauss smoothed EW images are shown in Fig. 4. We note that the Si EW image is relatively statistically stronger than the other two because of the high X-ray intensity, and the S map is slightly weak for the low photon statistics.

The EW images for Mg, Si & S lines display again the SE-NW elongated morphology which is also seen in the broadband and narrow-band images. The metal emission appears clumpy, too, with the gas structure seen in the broad- and narrow-band images. Many bright knots or clumps appearing in the broadband images (CSSW04), such as those located at around (18^h49^m39^s.4, -00°58'38'') (region #1), (18^h49^m39^s.6, -00°56'43'') (region #2), (18^h49^m27^s.3, -00°54'06'') (region #3), (18^h49^m29^s.3, -00°56'42'') (region

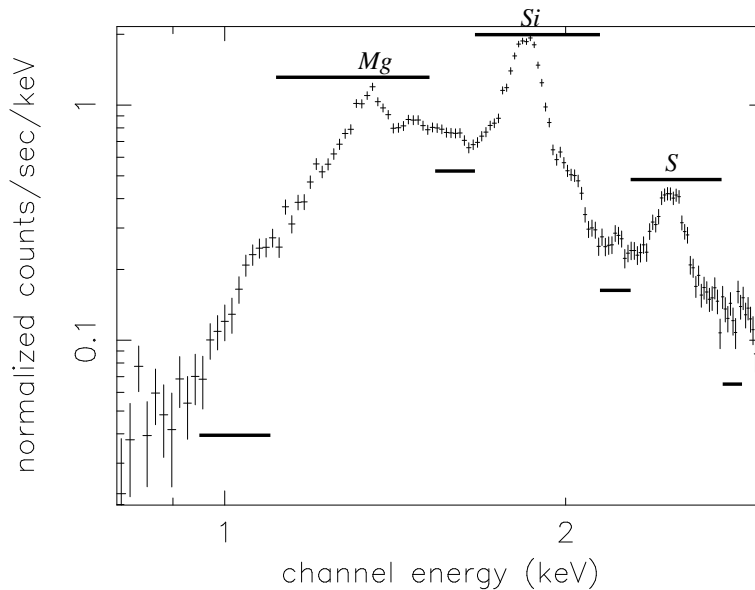


Fig. 2 The *Chandra* ACIS spectrum of the entire remnant. Horizontal bars above the spectrum, which are labelled by element, show the energy intervals used for each EW image; bars below the spectrum show the intervals used for the continua (see table 1).

#6), ($18^{\text{h}}49^{\text{m}}32^{\text{s}}.9, -00^{\circ}56'58''$) (region #7), ($18^{\text{h}}49^{\text{m}}35^{\text{s}}.5, -00^{\circ}57'04''$) (region #8), and ($18^{\text{h}}49^{\text{m}}29^{\text{s}}.8, -00^{\circ}57'45''$) (region #9), have their counterparts in the EW images. All these knots and clumps have been found to be of solar abundance (CSSW04), therefore the clumpy line emission revealed by the EW maps would arise from the clumpy interstellar medium (ISM).

It is interesting that the SW finger-like feature appears clearly in the EW maps of Si and S lines (Fig. 4b, 4c). A very faint hint of the Mg emission at the site of the protrusion is marginally discerned (Fig. 4a). Furthermore, the shape of the “finger” in the image for Si (Fig. 4b) bears a close resemblance to that in the smoothed broadband image (Fig. 1b). For comparison, we display the unsmoothed EW image for Si including the SW finger-like feature in Fig. 1c. In Fig. 1c, this protruding structure is measured to extend about $1.3'$ (approximately 3 pc at a distance 8 kpc) outside the radio shell. We note that the EW maps depend not only on the element abundances but also on the temperature and on the ionization age, so that the given EW images should only be taken as an indication of some feature which represent the position and brightness of line emission but not the actual maps of the mass distribution.

4 DISCUSSION

We have seen that both the narrow-band and EW images show similar clumpy structure interior to the remnant and the finger-like feature in Si and S protruding radially outside

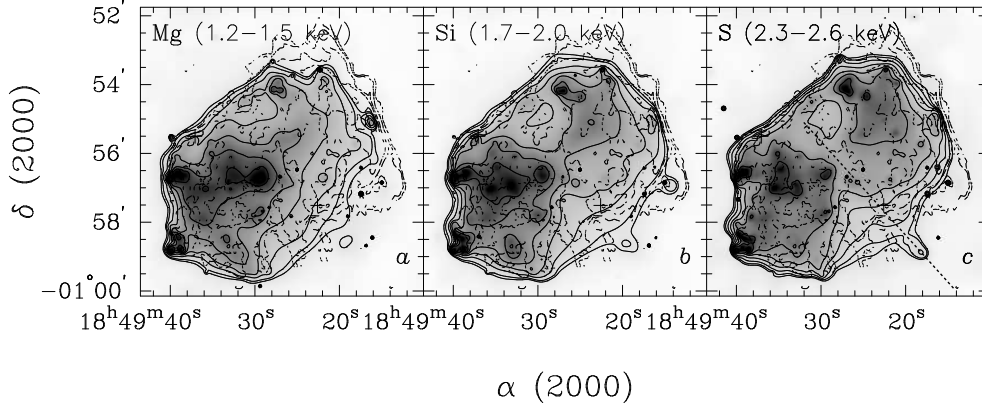


Fig. 3 Adaptively smoothed narrow band 1.2-1.5, 1.7-2.0, and 2.3-2.6 keV (including Mg He α , Si He α , and S He α , respectively) diffuse emission images (with S/N ratio of 3) overlaid with the dashed contours of 1.5 GHz radio emission (at 1.5, 3.19, 8.25, 16.69, 43.68, and 62.24×10^{-3} Jy/beam) (Moffett & Reynolds 1994). The seven levels of solid contours are plotted with square-root intensity scales between the maximum and the 15% maximum brightness. The two plus signs in each panel denote the OH maser points (Frail et al. 1996). The dotted line in (c) roughly indicates the symmetrical axis of the SW protrusion.

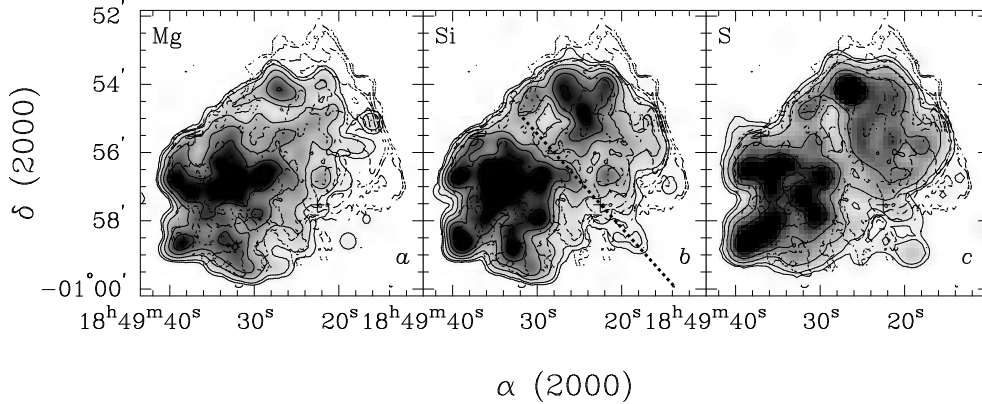


Fig. 4 EW images of Mg, Si, and S lines. The Mg and Si (S) images are extracted with $4''$ ($8''$) pixels and smoothed by a Gaussian with $\sigma = 12''$ ($16''$). The seven levels of solid contours are plotted with square-root intensity scales between the maximum and the 3% maximum brightness. These images are overlaid with the dashed contours (with the same levels as in Fig. 3) of 1.5 GHz radio emission (Reynolds & Moffett 1993). The two plus signs in each panel denote the OH maser points (Frail et al. 1996). The dotted line in (b) roughly indicates the symmetrical axis of the SW protrusion.

Table 1 Energy Bands Used for Generating the Equivalent-Width Images

Elements	Line (eV)	Low (eV) ^a	High (eV) ^a
Mg(Fe L)	1160-1560	950-1150	1570-1670
Si	1680-2050	1570-1670	2100-2250
S	2330-2730	2100-2250	2740-2840

^a The low- and high-energy bands around the selected line energies used to estimate the underlying continua.

the southwestern radio border. The gas clumps have a normal abundance according to CSSW04 and thus are essentially of interstellar origin. The most intriguing phenomenon unveiled here is the finger-like structure which is coincident with the “spill-out” portion seen in the broadband image (CSSW04). Limited by the insufficient counts of the spectrum that is extracted from the faint SW protruding region, we cannot make a spectral fit to decide the metal abundances. However, the similarity to the protruding feature of Si and other elements in Cas A may lend us a good clue to a possibility for the physical nature of the finger-like feature in 3C 391.

The finger-like protruding feature on the SW seen in the Si and S EW maps (Figs. 1c, 4b, and 4c) and in the narrow-band maps (Figs. 3b, 3c) is, to some extent, similar to the NE jet-like Si structure recently found in the famous SNR Cas A (Hwang et al. 2000). In Cas A, the EW maps for Si and other elements show a breakout protrusion on the NE, which is explained as one of jets of ejecta extending outside of the blast shock (Hwang et al. 2000, 2003, and 2004). Hwang et al. (2004) further suggest that the jets of ejecta in Cas A be yielded by an asymmetric supernova explosion of a collapsar with normal explosion energy ($2 - 4 \times 10^{51}$ ergs). The asymmetric structures in Cas A are not erased by the much less massive hydrogen envelope at explosion compared to SN 1987A, another core-collapse supernova exploded asymmetrically (Wang et al. 2002 and references therein), where the jets may have been erased by the hydrogen envelope (Chevalier & Soker 1989).

The association of SNR 3C 391 with a dense molecular cloud (Wilner et al. 1998; Reach & Rho 1999) makes it very likely for this remnant to result from an SN explosion of a massive core-collapse progenitor star, although no stellar remnant has been found yet (CSSW04). The possibility for two point sources (J184925.9–005628 and J184927.0–005640) located in the center and a bright unresolved point-like source (J184922.3–005334), with a power-law spectrum, near the NW boundary to be candidates of the stellar remnant can not be ruled out (CSSW04). Thus we suggest that the finger-like feature in Si and S lines in 3C 391 be probably caused by the jet of ejecta of the massive progenitor. Hence, like the case of Cas A, there might only be low mass hydrogen envelope at explosion of 3C 391, which has not erased the jet of ejecta. Heger

et al. (2003) and Chevalier (2005) suggest that stars with a mass of $10\text{-}25M_{\odot}$ will explode with most of their hydrogen envelope present. Therefore, if the jet-like structure in 3C 391 is true, the progenitor star might have a mass not less than $25M_{\odot}$.

Because of the irregular morphology of this remnant, the SN explosion site has not been clear yet. Reynolds & Moffett (1993) suggest that the explosion site be located within the northwestern half which is embedded by the dense cloud. If the symmetric axis of the protruding feature could indicate the trajectory of the ejection, then the explosion site may roughly be aligned with it. We plot such an axis in Fig. 3c and 4b and thus see that the explosion site may be located slightly northwestward from the remnant's geometrical center.

By comparison, the SW finger-like protrusion in SNR 3C 391 extends $3.5'$, about 8 pc at a distance 8 kpc, from the explosion site or the geometrical center of the remnant, longer than the X-ray jets of ejecta in Cas A, which measure exceeding $3.5'$, about 3.5 pc at a distance 3.4 kpc (Hwang et al. 2004). The fast-moving ($\sim 1.2 \times 10^4 \text{ km s}^{-1}$) knots along the jets of Cas A reach as far as $4.5'$ ($\sim 4.5 \text{ pc}$) from the center (Fesen 2001). If the protruding feature in 3C 391 indeed indicates a jet of ejecta, this contrast of lengths could be reasonable in view of the different ages and ambient gas densities of the two remnants. 3C 391 is estimated to be in an age of $\sim 4 \times 10^3 \text{ yr}$ (CSSW04) much larger than Cas A's age $\sim 320 \text{ yr}$ (Fabian et al. 1980), meanwhile one should note that the ambient gas density of 3C 391 ($\sim 30 \text{ cm}^{-3}$) is much higher than that of Cas A ($\sim 3 \text{ cm}^{-3}$) (Laming & Hwang 2003). One could naturally expect that the jets in Cas A could extend longer than 4.5 pc at an older age with a considerable deceleration.

The nature of the finger-like feature, especially the abundances of the metal species in this region, should be further investigated with a deeper X-ray exposure of one of the space missions.

5 CONCLUSION

We have constructed the narrow-band and EW images of SNR 3C 391 for the emission lines of Mg, Si, and S using the *Chandra* ACIS observational data. These images display a clumpy spatial distribution of metal species Mg, Si, and S within an elongated periphery of the supernova remnant, similar to the structure seen in the broadband images, suggestive mainly of interstellar origin. The most intriguing result is the finger-like protrusion revealed in Si and S lines on the SW border. A comparison is made between this protruding feature and the X-ray jets of ejecta seen in lines of Si and other species in SNR Cas A. The similarity between these features may suggest a possibility that the SW protruding finger-like feature in SNR 3C 391 be a trace of the jet of ejecta of an asymmetric core-collapse supernova explosion of a massive ($\gtrsim 25M_{\odot}$) progenitor star.

Acknowledgements We thank the anonymous referee for valuable advices. We also thank Jasmina, Lazendic and Bing Jiang for the help in the EW map production. This work is supported by NSFC Grants 10073003 and 10221001 and CMST Ascent Project Grant nkbrsf-g19990754.

References

- Chen Y., Slane P. O., 2001, *ApJ*, 563, 202
Chen Y., Su Y., Slane P. O. et al., 2004, *ApJ*, 616, 885 (CSSW04)
Chevalier R. A., 2005, *ApJ*, 619, 839
Chevalier R. A., Soker N., 1989, *ApJ*, 341, 867
Fabian R. C., Willingale R., Pye J. P. et al., 1980, *MNRAS*, 193, 175
Fesen R. A., 2001, *ApJS*, 133, 161
Frail D. A., Goss W. M., Reynoso E. M. et al., 1996, *AJ*, 111, 1651
Green A. J., Frail D. A., Goss W. M. et al., 1997, *AJ*, 114, 2058
Heger A., Fryer C. L., Woosley S. E. et al., 2003, *ApJ*, 591, 288
Hwang U., Holt S. S., Peter R., 2000, *ApJ*, 528, L119
Hwang U., Laming J. M., 2003, *ApJ*, 597, 362
Hwang U., Laming J. M., Badenes C. et al., 2004, *ApJ*, 615, L117
Laming J. M., Hwang U., 2003, *ApJ*, 597, 347
Moffett A. A., Reynolds S. P., 1994, *ApJ*, 425, 668
Park S., Roming P. W. A., Slane P. O. et al., 2002, *ApJ*, 564, L39
Park S., Burrows D. N., Garmire G. P. et al., 2003, *ApJ*, 586, 210
Reach W. T., Rho J. H., 1998, *ApJ*, 507, L93
Reach W. T., Rho J. H., 1999, *ApJ*, 511, 836
Reynolds S. P., Moffett D. A., 1993, *AJ*, 105, 2226
Rho J. H., Petre R., 1996, *ApJ*, 467, 698
Yusef-Zadeh F., Wardle M. et al., 2003, *ApJ*, 585, 319
Wang L., Wheeler J. C., Höflich P. et al., 2002, *ApJ*, 579, 671
Wilner D. J., Reynolds S.P., Moffett D.A., 1998, *ApJ*, 115, 247